

Optimisation of a nano-positioning stage for a Transverse Dynamic Force Microscope

S.C. Burgess*, G. De Silva*, T. Hatano*, S.G. Khan*, K. Zhang*, T. Nguyen***, G. Herrmann*, C. Edwards***, and M. Miles**

**Department of Mechanical Engineering, University of Bristol, University Walk, Bristol, BS8 1TR, UK;
{s.c.burgess@bristol.ac.uk, g.herrmann@bris.ac.uk}*

***Centre for Nanoscience and Quantum Information, University of Bristol, Tyndall Avenue, Bristol, BS8 1FD, UK*

****College of Engineering, Mathematics and Physical Sciences, University of Exeter, EX4 4QF, UK.*

Abstract: This paper describes the optimisation of a nano-positioning stage for a Transverse Dynamic Force Microscope (TDFM). The nano-precision stage is required to move a specimen dish within a horizontal region of 1 micron×1 micron and with a resolution of 0.3 nm. The design objective was to maximise positional accuracy during high speed actuation. This was achieved by minimising out-of-plane distortions and vibrations during actuation. Optimal performance was achieved through maximising out-of-plane stiffness through shape and material selection as well optimisation of the anchoring system. Several shape parameters were optimised including the shape of flexural beams and the shape of the dish holder. Physical prototype testing was an essential part of the design process to confirm the accuracy of modelling and also to reveal issues with manufacturing tolerances. An overall resonant frequency of 6 kHz was achieved allowing for a closed loop-control frequency of 1.73 kHz for precise horizontal motion control. This resonance represented a 12-fold increase from the original 500 Hz of a commercially available positioning stage. Experimental maximum out-of-plane distortions below the first resonance frequency were reduced to from 0.3 to less than 0.05 microns for the final practical prototype.

Keywords: design optimisation, prototype testing, FEA, atomic force microscope

1. Introduction

1.1 The need for design optimisation of Atomic Force Microscopes

Since its invention in 1986 [1], atomic force microscopes (AFMs) have become one of the most important tools to measure the 3-D topography of nano-scale objects including both biological and non-biological specimens [2][3][4]. The resolution of AFMs can be better than 1 nanometre (1×10^{-9} m) enabling measurements of specimens such as DNA and proteins [5]. AFMs are widely used for biomedical analysis in cancer research [6], cell biology research [7] and material science [8].

AFMs have a number of advantages over scanning electron microscopes (SEMs) such as the ability to carry out 3D scanning, the ability to scan untreated specimens and the ability to scan without the need for a vacuum. However one of the key disadvantages of AFMs is relatively slow scanning rates. This is restricting the usefulness of AFMs in many areas of research. In particular AFMs are generally not able to scan processes in real time.

This paper deals with the optimisation of the positioning stage of an advanced type of atomic force microscope called a transverse dynamic atomic force microscope (TDFM). A TDFM has higher accuracy and the capability to scan softer specimens [9]. However, as with other types of AFM, TDFMs suffer from slow scan rates. In addition their resolution can be limited when scanning rates are high. Therefore there is a need for design optimisation of TDFMs to achieve improved levels of resolution and speed of scanning. In particular, the positioning stage, which moves the sample under the probe, is a critical component that limits the speed and accuracy of operation.

1.2 Introduction to the Transverse Dynamic Force Microscope

The basic layout of a TDFM is shown in Figure 1. The specimen to be examined is placed on a thin specimen dish within a nano-positioning stage that can be moved in a horizontal x-y plane. Conditions must be such that the specimen is covered with a microscopic water layer as this is required for the scanning process. In ambient conditions, a specimen is always covered with a thin water layer due to general humidity at room temperature and pressure (21°C, 100kPa).

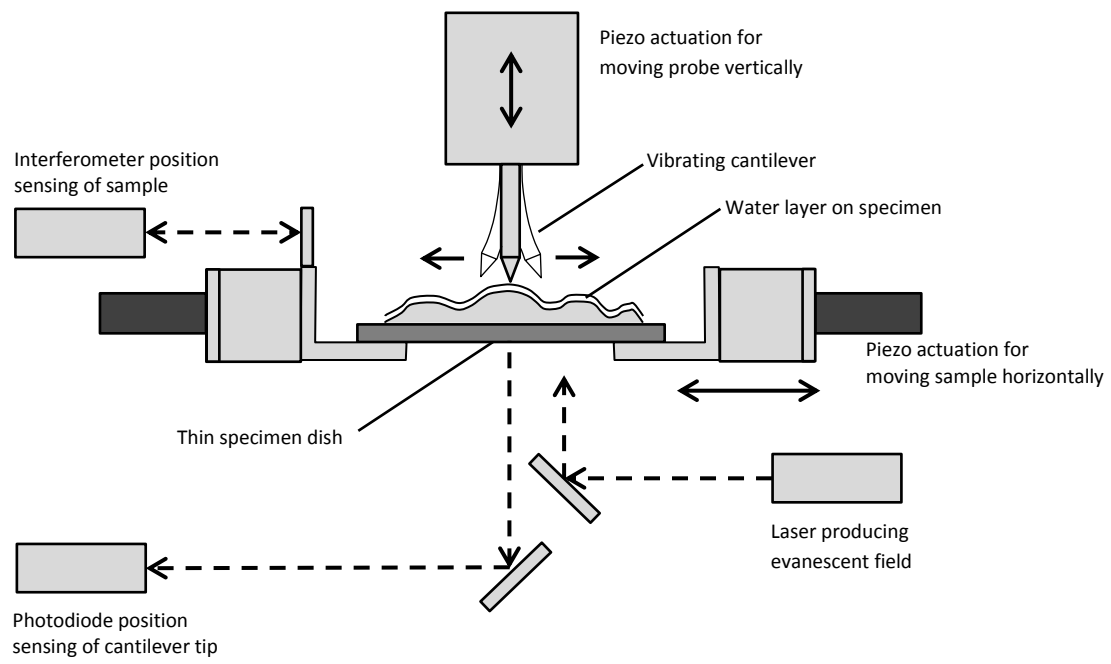


Fig. 1: Schematic of the TDFM layout

A TDFM uses a vertically oriented cantilever probe which is different to the horizontally orientated probes of traditional AFMs [9][10][11][12][13]. The vertical cantilever is vibrated at a set frequency and placed above the specimen in close proximity such that there is interaction between the cantilever and the molecules of water within the microscopic water layer that covers the specimen.

When the cantilever interacts with the water layer the vibration is damped and the amplitude of vibration is decreased. The exact amplitude of vibration is dependent on the level of penetration in the water layer. During scanning, if the probe is moved in the vertical axis such that the amplitude of vibration is constant then the probe follows the profile of the specimen. This principle of interaction with the water layer above the specimen enables non-contact scanning.

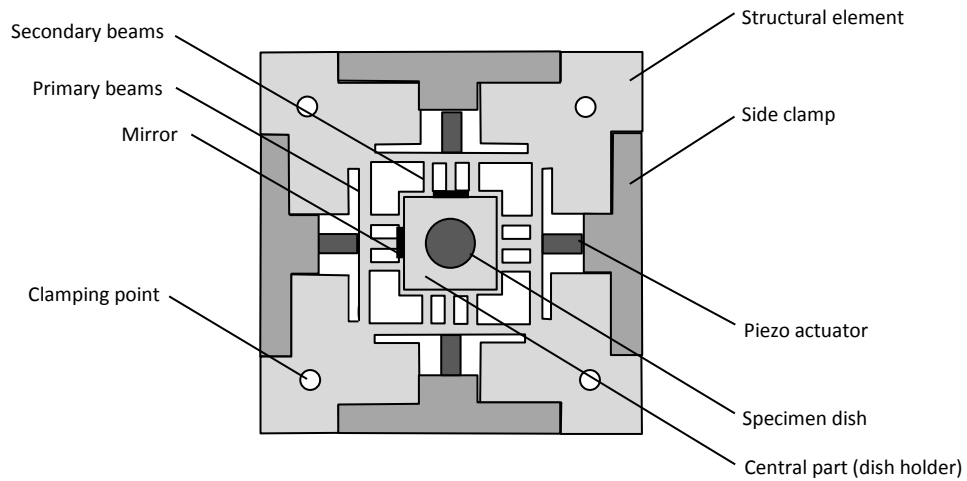
The change in vibration of the probe is measured by a laser optical detection system, which is set beneath the thin specimen dish underneath the specimen. The optical detection system creates scattered evanescent electromagnetic waves in the surrounding area of the specimen [14]. The reflected component of these is detected by a photo-detection system to obtain a measurement of the cantilever tip oscillation.

1.3 Introduction to the nano-positioning system

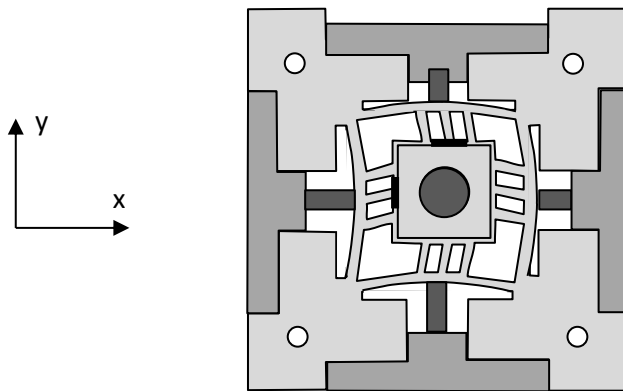
The layout of the positioning stage is shown in Fig. 2a and is based on a concept produced by Schitter et al. 2006 [15]. The nano-positioning stage consists of:

- A structural element
- A central circular specimen dish
- Four piezo actuators
- Four side clamps
- Two mirrors

The structural element itself consists of a number of separate features including four primary flexural beams; twelve secondary flexural beams; a central dish holder, two mirror holders; and four anchor points.



(a) Layout of positioning stage



(b) Example of x and y movement of the dish holder via flexing of structural beams

Fig. 2: Assembly of the positioning stage

The primary beams are deflected directly by the adjacent piezo actuator as shown in Fig. 2b and allow a deflection of 1 micron in the x and z axes. The secondary beams allow simultaneous movement of the dish in x and y directions. The combination of primary and secondary beams give the required stiffness.

Piezoelectric actuators are used because of their high stiffness, linear displacement and high load capacity. A laser-interferometer system is used to detect movement in the x and y axes, as it gives a high positioning accuracy of 0.3 nm.

There are two vertical mounts (flags), one on each axis, protruding from the edge of the specimen holder. They are used for the attachment of thin mirrors, acting as reflectors for the two laser beams of the laser interferometer. The ‘T shaped’ side clamps are used to apply/adjust the mechanical preload applied to the piezo actuators.

1.4 Performance of TDFMs

The main measures of technical performance are scan accuracy and speed. These are very closely linked to two physical properties: (i) the natural frequency of positioning stage and (ii) the out-of-plane distortions of the stage during in-plane movement. Higher natural frequencies result in a higher bandwidth and hence scan rates. Low out-of-plane distortions mean that the accuracy is better for both stage position measurement and probe position measurement.

1.5 Design constraints and objectives

The positioning system has the following constraints and requirements:

- The design space for the structural element is 93 mm x 93 mm x 9 mm.
- The dish holder must be able to displace up to 1 micron in the x and y axes
- The stage must hold a specimen holder disc of 18 mm diameter.
- The design space for the specimen dish is shown in Fig. 3

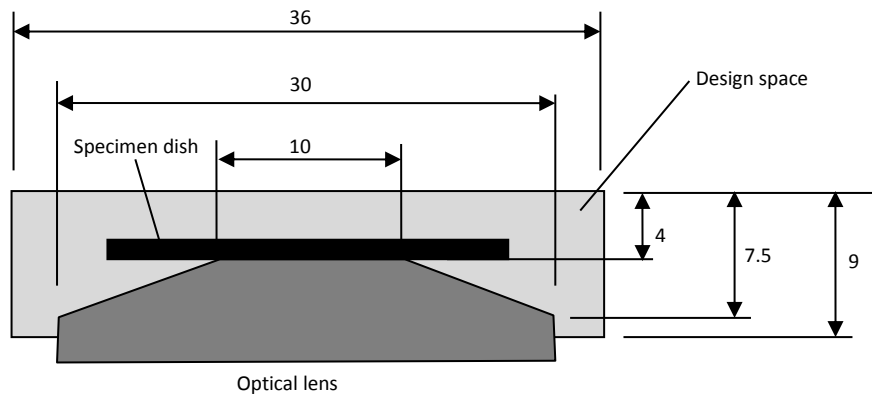


Fig. 3: Design space for the central dish holder

The overall design objectives for the nano-positioning stage are:

- lowest natural frequency > 6000 Hz
- experimental out-of-plane displacements < 0.05 micron (for 1 micron x and y in-plane movement; corresponds to a -25 dB gain for out-of-plane to in-plane displacement.)

1.6 Current performance of TDFMs

For the first prototype we used the high precision stage of the Physik Instrumente, P-733.2, [16]. This had a minimum resonance of 500 Hz which limited the bandwidth of any motion to less than 300 Hz, although account should be taken that it has a relatively large motion range of 100 microns. Other commercial precision stages for this purpose have at best resonance frequencies at about 2000 Hz [17]. Therefore significant design optimisation was required to meet the design goals.

2. Conceptual design of a new positioning stage

2.1 Existing designs

Some of the main types of positioning stage geometries are shown in Table 1. An example of the comb-flexure concept is given by Schitter et al [15] and involves direct and symmetric loading. An example of a hybrid flexure is given by Yong et al [18] and involves indirect loading but a symmetric flexure layout. An example of a stage with direct loading and asymmetric layout is given by Polit et al [19]. In each case the structures are designed so that the maximum displacements do not involve axial stiffening in the beams.

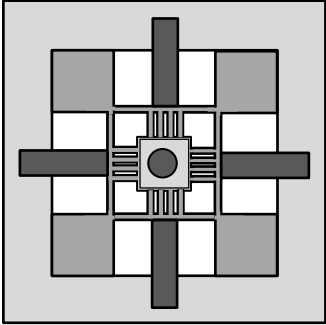
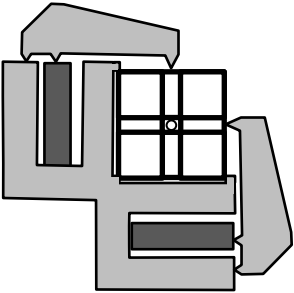
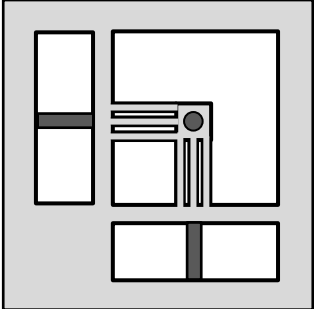
Concept	Features
	<ul style="list-style-type: none"> ➤ Symmetrical comb-flexures ➤ Direct and symmetrical loading <p>The push-pull motion of the actuators involves a more complex actuation but has the advantage of producing a higher preload</p> <p>The direct loading of the actuators on to the flexural beams results in a higher stiffness of the overall system</p>
	<ul style="list-style-type: none"> ➤ Symmetrical beams ➤ Indirect and asymmetrical loading <p>The design is not space efficient and the pivot points reduce stiffness</p>
	<ul style="list-style-type: none"> ➤ Asymmetrical flexures ➤ Direct and asymmetrical loading <p>The direct loading of the actuators onto the flexural beams results in a higher stiffness of the overall system</p> <p>The overall system is not space efficient</p> <p>Low out-of-plane stiffness due to the overhang of the central part</p>

Table 1: Main types of positioning stage geometries

2.2 Shape selection of new stage

The basic concept for the structural element of the new positioning stage is shown in Fig 4. It adopts the direct-loaded and symmetric layout of Schitter et al [15] because of the efficiency and simplicity of the design. However there is an additional ‘undercut’ added to increase the length of the primary beams. The increase in length means that the beam thickness can be increased which improves out-of-plane stiffness.

The outside geometry of the structural element is determined by the clamping points, the side clamps and piezo actuators. In addition, the stage must have a means for holding a central dish. However, there is freedom to change and optimise the shape of the stage between the dish interface and the outside constraints. The main internal features can be divided into three areas:

(1) *Primary flexural beams:* The primary flexural beams are maximised in length to minimise stresses during deformation.

(2) *Secondary flexural beams:* There are three secondary flexural beams attached perpendicular to the primary beams. One reason for having multiple beams is that the stresses are lower for multiple beams in comparison to a single beam of the same stiffness. This is because the individual beams of a multi-beam layout are more slender (lower y) and this leads to lower stresses because stress is a function of Ey/R where E is Young’s Modulus, y is the distance to the neutral axis and R is the radius of curvature. Another advantage of multiple secondary beams is that they increase the out-of-plane stiffness of the central part of the stage by minimising the amount of overhanging sections of material. The reason for selecting three beams (and not more) was to keep manufacturing complexity down. But there would potential be slightly higher performance from having more than three beams.

(3) *Central dish holder:* The first design iterations started with a square dish holder that was not symmetrical in the Z axis. A circular shape was explored in the design optimisation as well as increased symmetry in the Z axis. The central dish holder also has two mirror holders that must be able to support mirrors for position sensing.

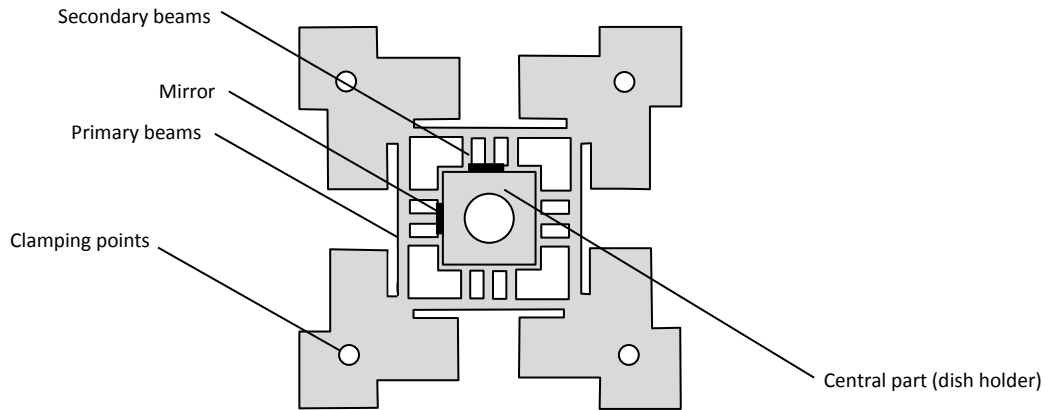


Fig. 4: Structural element of the positioning stage

2.3 Material selection

The natural frequency of a simple spring-mass structure is given by

$$\omega = \sqrt{k/m}$$

In terms of material properties, the natural frequency of a simple spring-mass structure is a function of

$$\omega = f(\sqrt{E/\rho})$$

Therefore the best material for achieving high frequency is the one with the highest value of

$$\sqrt{E/\rho}.$$

There is an additional advantage in having a high Young's modulus because a higher modulus allows thinner sections to be made. The reason for this is that the thickness of thin sections is limited by buckling performance and buckling performance is directly proportional to the material modulus. The advantage of thinner sections is that it is possible to produce more intricate shapes that put more material away from the neutral axis thus increasing the second moment of area.

The main candidates for the position stage are steel, aluminium and titanium. Their performance is shown in Table 1, which also shows the linear thermal coefficients. Carbon Fibre Reinforced Plastic was not considered because of manufacturing limitations.

	E GPa	ρ kg/m ³	$\sqrt{E/\rho}$	Thermal Coefficient α $\mu\text{m}/(\text{K}\cdot\text{m})$	Rank frequency	Rank modulus	Rank Thermal Expansion
Steel	193	8080	4887	10.8	3	1	2
Aluminium	69	2710	5042	23.1	2	3	3
Titanium	114	4043	5310	8.1	1	2	1

Table 2: Material properties for selection of stage material

The results in Table 2 show that steel is ranked third behind titanium and aluminium for frequency. However, there is only around 8% difference between titanium and steel so the range of performance for $\sqrt{E/\rho}$ is not that large. In terms of buckling performance, which is indicated by Young's modulus, steel is ranked first by a large margin. Therefore, steel was chosen because of its ability to form thin sections whilst still achieving a comparable frequency performance to other materials. This, is also confirmed by the fact that titanium and steel have similarly low thermal expansion coefficients, while Aluminium is more than twofold the value of titanium and steel.

2.4 Actuator and actuator layout selection

A schematic of the actuator layout is shown in Fig. 2. The actuators act in parallel with the structure. Piezo-actuators are a good choice for microscope positioning systems because of their high accuracy and high stiffness. Piezo-actuators were chosen that could fit into the space available whilst giving the maximum force. By maximising the actuator force this enabled the stiffness of the stage to be maximised for a given displacement. The piezo-actuators stiffness is around 18% of the stage stiffness so they add a significant amount of extra stiffness. A push-pull layout is chosen because this gives more symmetry to the displacement and enables a higher preload.

2.5 In-plane stiffness and preload selection

To maximise natural frequency, it is necessary to maximise in-plane stiffness. However, the stiffness is limited by the requirement for the actuators to displace the structural element by 1 micron in the x and y directions. Therefore actuators were chosen that could maximise force

in the space available. The stiffness of the element was then maximised within the capabilities of the actuators.

Compressive preloads between the actuators and the structure are necessary to avoid backlash. They sum across the push-pull set-up. Hence, to compute for each actuator its own preload, for the chosen actuator arrangement (two P-885.11 actuators [20] for each direction) a blocking force of 400N needs to be considered. The maximum actuation voltage was $\pm 60\text{V}$ and a maximum unrestricted displacement of $4\ \mu\text{m}$ for the operating voltage of 60V (Fig. 5). To displace 1 micron the maximum preload is 300N. Therefore the preload was set at 300N. This resulted in a maximum in-plane stiffness of the structural element of $600\text{N}/\mu\text{m}$ (see also documents within [20]).

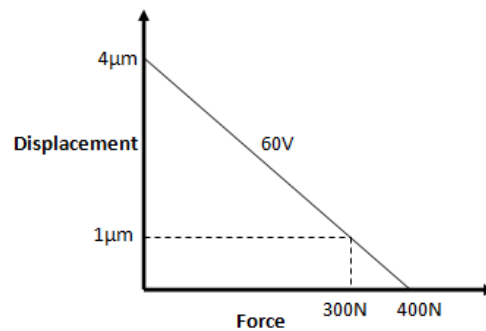


Fig. 5: Piezo actuators force to displacement relationship at 60V

This means that the structural element needed to be shaped such that the stiffness was $600\text{N}/\mu\text{m}$ in both x and y directions. Note that preloads are likely to change considering the thermal coefficient of steel (Table 1) and the piezo-actuator ($10.8\ \mu\text{m}/(\text{K}\cdot\text{m})$, [20] by 2.5% for a 1K change in temperature. This should be acceptable in a closed-loop raster scan scenario and considering the good temperature stability ($\sim 1\text{K}$ per hour) of the room for the TDFM system. A feedforward control combined with temperature sensing to adjust the preload voltage can be alternatively used.

2.6 Clamp selection

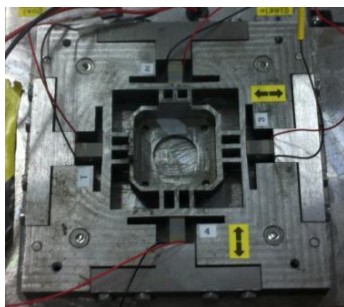
Clamping points to a rigid structure are important for achieving high frequencies. Four clamping points were chosen as shown in Figure 4. The clamps consisted of 3 mm diameter bolts tightened with a preload of 1.5 Nm.

3 Prototype 1 design and performance

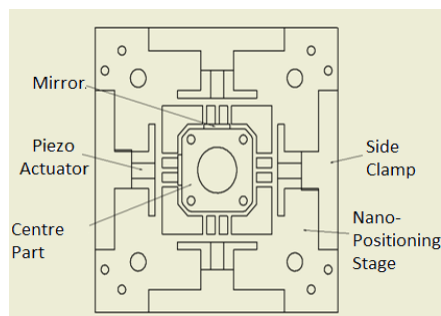
3.1 Design description and rationale

The nano-positioning stage was manufactured using stainless steel and is shown in Fig. 6. The piezo-actuators were preloaded with a 300N force through the application of 60V and in-plane displacements were achieved through push-pull motion of the actuators.

(a) 1st HighSpeed Stage Prototype



(b) 1st High Speed Stage's Schematic



(c) $\frac{3}{4}$ Section of the 1st High Speed Stage prototype showing z-axis assymetry

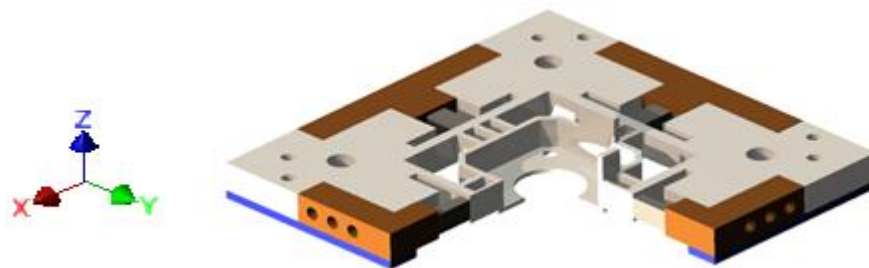


Fig. 6: High-speed-stage Prototype 1

3.2 Testing of structural performance

Practical Swept Sine System Identification was carried out for the first prototype, which excites the stage with sinusoidal signals at distinct frequencies within specific frequency ranges to obtain the frequency-dependent phase change and amplitude gains. A six-channel high speed piezo-drive amplifier with a voltage amplification gain of 15 (www.techproject.at) was used to drive the piezo actuators. The piezo-actuators were excited each in the X-direction and then in the Y-direction. For each excitation direction, the relevant in-plane X (or Y) translation at the flags and the vertical out-of-plane Z-motion at the centre part of the

stage were measured. Consequently, the frequency responses were obtained, identified with XX (excitation in X-direction and translational X-direction measurement), XZ (excitation in X-direction and translational Z-direction measurement), YY or YZ (Figure 7 for XX and XZ).

It should be noted that in computer modelling and physical testing there is no specimen dish in the stage. The dish is very thin (0.16mm) weighing around just 0.1 gram which is typically less than 0.4% of the stage mass and has no significant effect on the result.

The performance of the first prototype is summarised in Table 3.

	FEA	Experiment
Resonance (Hz)	7800	4500
Max out-of-plane displacements (μm) for 1 μm in plane motion	>1	0.3 (below resonance frequency)

Table 3: Summary of performance of prototype 1

Even though this stage achieved a high first resonance frequency of ~ 7.8 kHz, Prototype 1 generated a significant amount of out-of-plane vibrations in the Z direction once actuated in-plane. Figure 7 presents the amplifier input to translational output frequency Bode-plot derived from a swept sine analysis. It can be clearly seen that there is a difference between the in-plane and the out-of-plane motion of ~ 10 dB in low frequency which provides an equivalent relative gain factor of ~ 3.16 between the XX and XZ amplitude plot. Both the experimental and the FEA performance are not acceptable. The FEA out-of-plane vibrations present the worst case performance and are of similar magnitude as the desired in plane motion of 1 μm , while the experimental results focus on the performance below the resonance, assuming that a closed-loop control strategy will not excite the high frequency resonances.

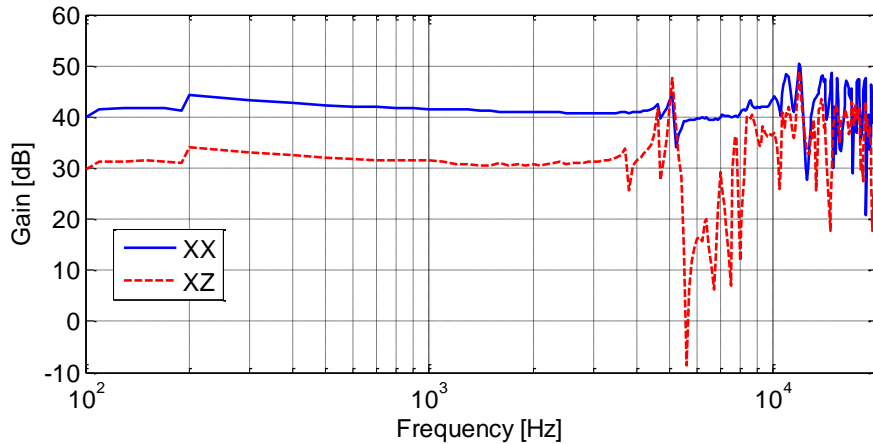


Fig. 7: Performance [nm/V] of the 1st high-speed-stage Prototype in the frequency domain using a high bandwidth piezo-amplifier with voltage gain of 15

3.3 Lessons from prototype 1

Even though the Prototype 1 stage obtains a resonance of over 7 kHz during the Modal Analysis, and ~5kHz during the actual sine sweep analysis, the operational bandwidth of the high-speed-stage is restricted to 2 kHz. This is due to the significant effect of the out-of-plane vibrations beyond this frequency. The lack of symmetry of prototype 1 across the X-Y plane in the dish holder inevitably causes out-of-plane distortions during x and y movements. Therefore, it was concluded that the next prototype should be designed with vertical symmetry. In addition, it was concluded that significant shape optimisation was required to meet the performance targets.

4. Prototype 2 design and performance

4.1 Physically idealised model and design development

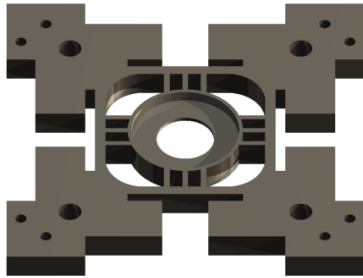
A new positioning-stage structure layout was developed using CAD and FEM. A CAD model was created for prototype 1 and correlated with test results to verify the validity of the model. This model was then used to test the effect of changes in structural shape on performance. Shape optimisation was carried out in two areas: (i) shape optimisation of the central dish holder; and (ii) shape optimization of the primary and secondary flexural beams.

Shape optimisation of the central dish holder

The first change in shape introduced was to replace the square central dish holder with a circular central dish holder. In addition, the asymmetry in the Z axis was replaced with a

symmetric cross section in the z axis as shown in Fig. 8. The dimensions were adjusted so as to give the required in-plane stiffness of 600N/ μm .

(a) Physically Idealised Model



(b) stage-centre-part with I beam cross section

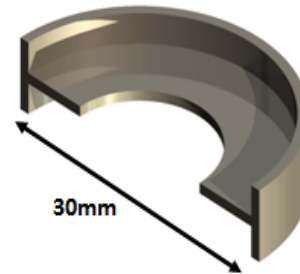


Fig. 8: Physically idealised model with the new Centre Part

The FEA of the physically-idealised-model was tested for its maximum piezo-actuator loading of 600N. The physically-idealised model demonstrated superior performance over the old high-speed-stage especially in terms of its resonance and out-of-plane displacements (Table 4). As the design assumes perfect symmetry of the physically idealised model, a vertical relative displacement of 1mm for the piezo-actuators is deliberately introduced for all following FEAs. This induces out-of-plane motion, which otherwise would not be observed in this design.

Resonance (kHz)	10,000
Max out-of-plane displacements (μm) for 1 μm in plane motion (FEA with intentionally introduced asymmetry of Piezo-actuator placement)	0.453
% increase of resonance	28%
% reduction of out-of-plane displacements	>55%

Table 4: FEA predicted performance of the physically-idealised-model

During the FEA, it was discovered that the centre part of both the old and the new high-speed stage deformed due to the piezo-actuator loading. This is undesirable because it can cause the specimen dish to slide over the centre part surface which itself brings errors into position measurements. Hence, it was necessary to strengthen the structure of the stage-centre-part in order to minimise deformations during actuation.

4.2 Shape optimisation of the central part dimensions

The phenomenon of a deformed stage-centre-part was further tested with FEA. From 300N to 600N there should be an overall displacement of 1 micron displacement of the centre of the dish with deformation between the two sides of the central part having a relative displacement of zero. However, when the preloaded stage was actuated from 100-600N and the predicted relative deformation was up to 0.841 microns. This modelling confirmed the need to stiffen the centre stage part.

Increasing the thickness of the base plate from 1mm to 3mm significantly reduced the deformation but also increased the mass of the stage-centre-part, and reduced the resonance bandwidth from 10 to 8.5 kHz. This thickness was chosen and the reduction of resonance was considered as an acceptable trade-off for the elimination of the measurement error.

Because the circular rim of the central part was only 1mm in thickness it was another key source of the relative deformation. Therefore a 45° chamfer was added as shown in Fig. 9 to increase the stiffness. This further change effectively removed the relative deformation but reduced the resonance by ~1kHz. However, this again was considered an acceptable trade-off.

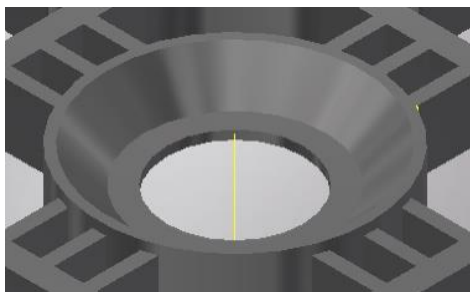


Fig. 9: Showing the 45 degree chamfer added to the circular ring

4.3 Shape optimisation of the primary and secondary beams

The chosen shape parameters of the primary and secondary flexural beams were T, G, W and L, as shown in Figures 10(a) and (b). Their dimensions were varied in a manual iterative process, whilst maintaining the constant in-plane stiffness of ~600N/ μm .

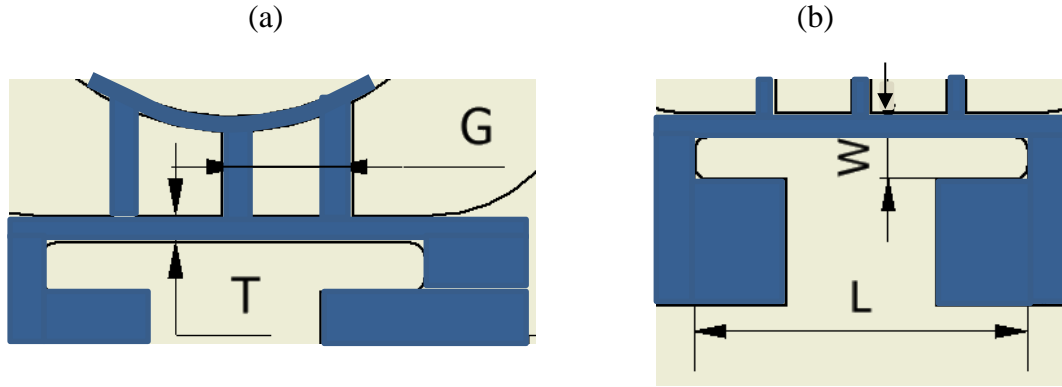


Figure 10: Identified features to tune the stiffness

It was observed that increasing the Gap W and L from their initial values of 2.5 mm and 22mm respectively decreased the in-plane stiffness of the high-speed-stage. During optimization, W was maintained at its initial value, and L was increased to 25mm in order to obtain an optimum in-plane stiffness of around 600 N/ μ m. Stiffness increases due to increasing G were compensated for by decreasing T .

Figure 11 demonstrates the variation of the resonance with Gap G while its stiffness is being compensated by combined changes of W and T . From these results, the optimum length of G was increased to 6mm, as the gradient of the curve is almost zero while its respective value for T was fixed at 1.87mm. This decision was further supported by the requirement of having the value of T greater than 1.5mm to provide enough structural spacing for the piezo-actuator-flexure boundary thereby preventing yielding. In fact, a minimum safety factor of 4 was maintained during this design process. These new dimensions increased the resonance from ~8.7kHz to ~8.95kHz.

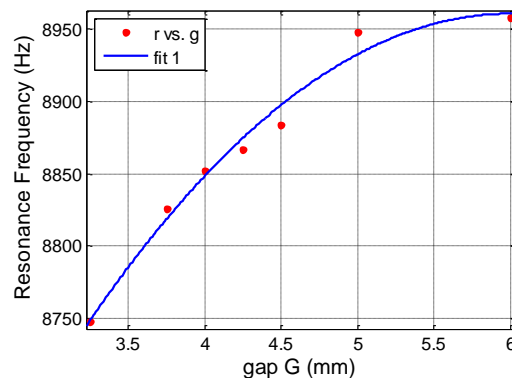
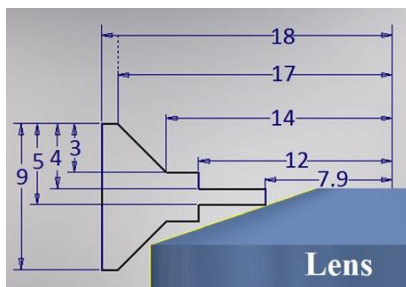


Figure 11: Resonance variation vs. gap G , keeping gap L constant

4.4 Shape optimisation- centre part re-design to fit the TDFM system

The stage-centre-part required some further re-adjustment in order for it to fit the actual optical TDFM setup. This is to avoid the surface of the optical lens (below the stage-centre-part) being in contact with the specimen dish. Perfect symmetry and chamfer profiles as shown in Figure 12 were maintained. Overall, the stage-centre-part diameter was increased from 30mm to 36mm.

(a) Stage-centre-part re-design



(b) New stage-centre-part cross section

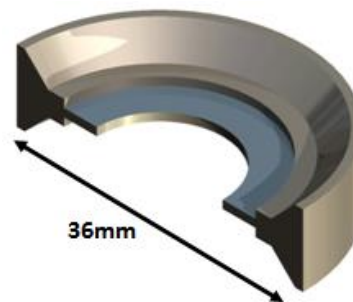


Figure 12: Re-design of the new centre part

The modified stage-centre-part can accommodate 18mm diameter circular specimen slides for operation. The new high-speed-stage flexure lengths were maintained, and its in-plane stiffness was tuned to approximately 600N/ μm by increasing L to 26mm.

This stage-centre-part enlargement further decreased the resonance from $\sim 8.9\text{kHz}$ to $\sim 7.3\text{kHz}$. A maximum out-of-plane displacement of $0.41\ \mu\text{m}$ was measured in FEA with a piezo-actuator misalignment as mentioned in Section 4.1 for a maximum 600N Piezo actuation.

A raised corrugated profile was tested on the high-speed-stage near the four bolt holes at the corners of the stage as seen in Figure 13a. This change increased the resonance frequency from 7.3 kHz to 7.65 kHz and L was increased to 26.5mm to retune the stiffness. This further reduced the out-of-plane displacements to $0.31\ \mu\text{m}$ in the FEA. This profile also acts as a bottom supporting mount/foot profile. It reduces the contact area for the high-speed-stage to sit on the slow micro-positioning stage of the TDFM. The use of the profile will be further discussed in Section 5.2.

Two mirrors for position measurement

In order for the laser to detect the high-speed-stage displacements, it is required to **have** two mirror holding flags on the stage centre-part. They are to be kept as close to the center as possible, while also accommodating room for the specimen slide. This is mainly to reduce the

measurement error based on the difference in displacements of the specimen slide and the mirror-holding flag. In order to reduce the complexity of the milling process during manufacture of the flags, 4 rectangular profiles were added to the stage-centre part which also supports the flags while maintaining symmetry across the XZ and YZ planes. The mirror holding flags were found to be rigid through the frequency bands of interest.

4.5 Evaluation of the CAD Model

The performance of the new high-speed-stage as observed in FEA (Fig. 13) is shown in Table 6. Again the same asymmetry in the piezo-actuator placement is used as for the result of Table 3.

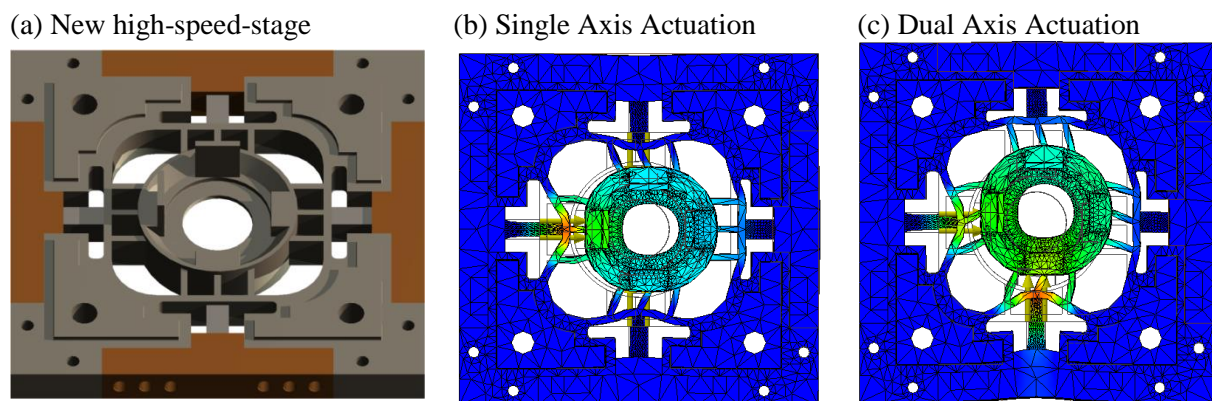


Fig. 13: New high-speed-stage design and its FEA

Resonance (kHz)	7140
Max out-of-plane displacements (μm) (FEA with intentionally introduced asymmetry of Piezo-actuator placement)	0.38
% increase of resonance	-8.5%
% reduction of out-of-plane displacements	>62%

Table 6: FEA predicted performance of the new high-speed-stage

5. Prototype 2 dynamic tests

5.1. Initial test results

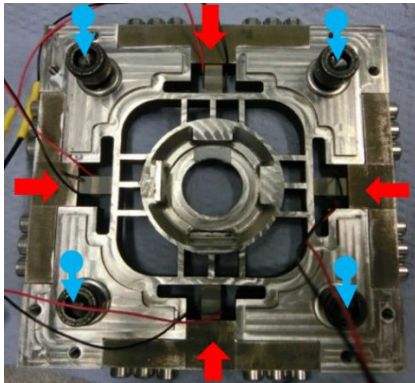
After manufacture of the prototype 2 stage (Fig. 14), the frequency based system identification (as in Section 3.1) was carried out for the high-speed-stage. The high-speed-stage was first tested on a steel block mimicking the operation of the actual TDFM with bolts. Initial test results revealed sensitivity to preload conditions as shown in Fig. 15. In addition,

the best preload conditions had a performance far inferior to that predicted by FEM.

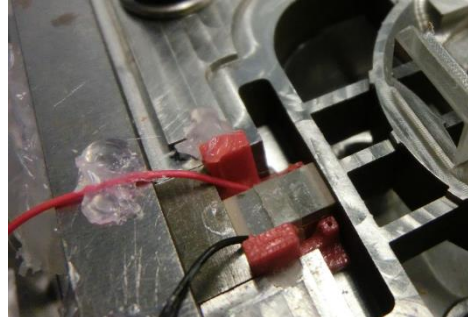
(a) New high-speed-stage

(↓ = side preload)

(↓ = vertical preload)



(b) Piezo actuator alignment with aligner



(c) Piezo actuator aligner

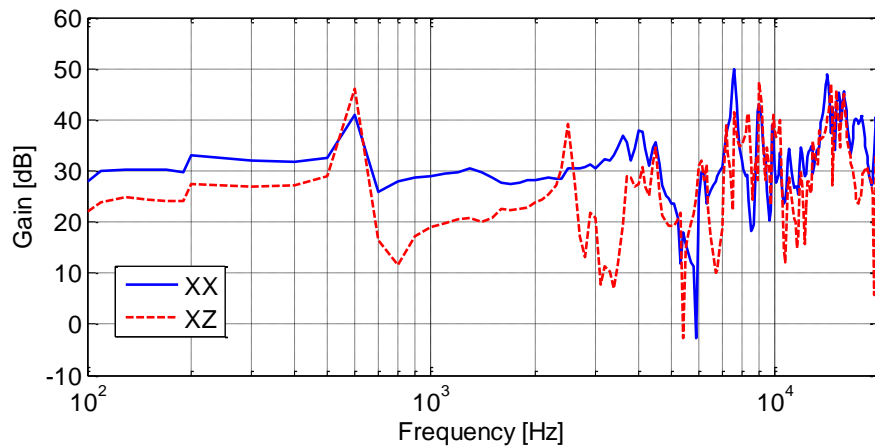


Fig. 14: Manufactured high speed nano positioning stage and piezo actuator alignment

The preloads were produced and measured by use of a digital torque wrench with a 0.5 – 5 Nm range. The bolts were gradually tightened in sequence so that the pressure was built up uniformly over the whole stage. Initially, the best performance was observed with condition B where both the side clamp and vertical bolt preloads were high. The resonance was observed at a frequency of ~6kHz and the maximum out-of-plane displacement was 0.3 microns (~10dB lower than its respective in-plane motion).

It can be observed that there is a significant improvement in resonance when the vertical preload torque was increased from 0.5 to 2 Nm. This is mainly because it increased the vertical stiffness, thereby firmly holding the high-speed-stage to the base. But still the out-of-plane movements are considerably higher than predicted with the FEA model.

(a) Condition **A**: Low vertical & high side-clamp preloads



(b) Condition **B**: High vertical and high side-clamp preloads

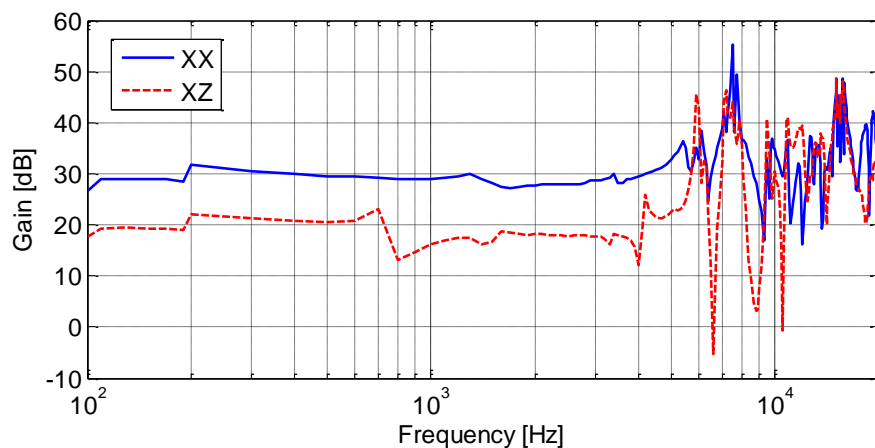


Fig. 15: Initial high-speed-stage performance [nm/V] for different preload conditions using a high bandwidth piezo-amplifier with voltage gain of 15

5.2. Possible causes for decreased performance of physical prototype

5.2.1. Uneven bottom surface

It was suspected that the high-speed-stage bottom foot profile surface was not sufficiently flat (Fig. 16) and that this was introducing unwanted compliance into the system. In order to investigate this possibility, a thin film of red ink was coated to the bottom foot profile of the high-speed-stage and its footprint was taken on a white sheet of paper.

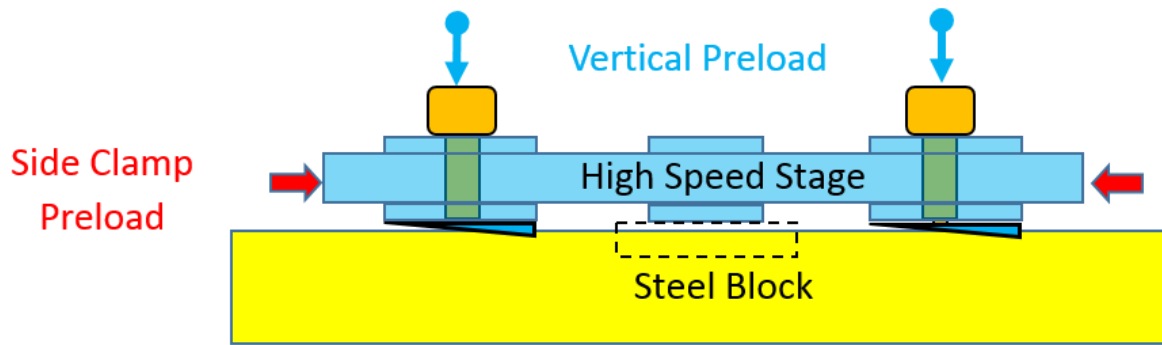


Fig. 16: Schematic of the high-speed-stage test system

As seen in Figure 17, the four foot profiles of the high-speed-stage are not level with each other. The no. 3 foot profile is clearly flatter than the rest of the profiles. The no. 4 foot profile has least contact with the paper. Therefore, the high-speed-stage tends to vibrate around its contact points when the vertical preloads are low. A lack of flatness of the positioning stage causes bending moments to be generated during preloading and these cause unwanted distortions.

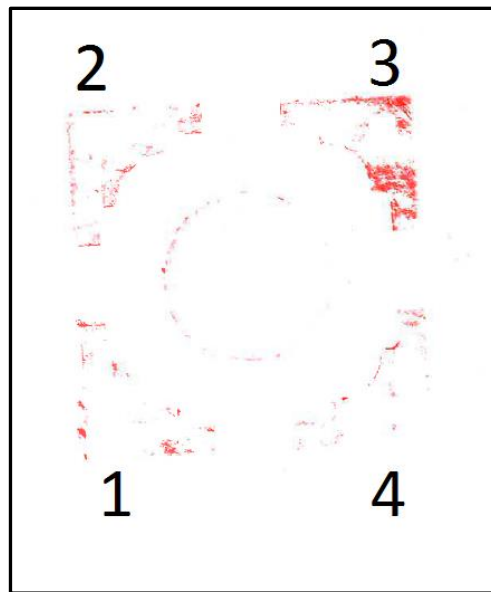


Fig. 17: Unlevelled footprints of the high-speed-stage

5.2.2. Misalignment of the piezo actuators

Another major reason for higher out-of-plane displacements is due to misalignments of the actuating piezo-actuators as these misalignments degrade the symmetry of the high-speed-stage. There was also gradual misalignment of the piezo-actuators with successive actuation. This has been observed although the side clamp preloads were controlled. The use of the piezo actuator also causes the side clamps to vibrate so that the bolts loosen. Therefore, these loose bolts may have to be retightened for each successive test.

5.3. Counter measures to improve on initial tests

5.3.1. Levelling of the bottom foot profiles

Two options were considered for solving the flatness problem. One was to create a three-point kinematic interface and a second was to carry out a careful grinding process to create an ultra-flat interface. A kinematic connection was not chosen because the stage has four-part symmetry and does not easily lend itself to a three-point connection. Therefore the ultra-flat machining solution was pursued.

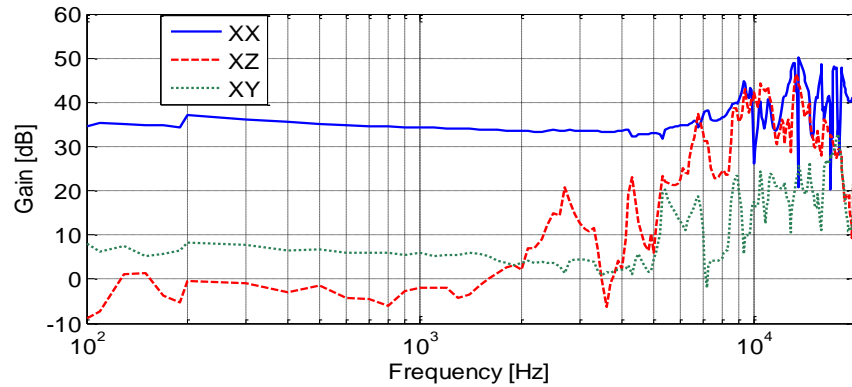
After the first tests, the bottom foot profiles of the high-speed-stage were carefully ground so that the foot profiles were almost 100% flat and in level with each other. Similarly, the top surface of the steel block used for the high-speed-stage has also been ground so that the surface area of the high-speed-stage foot profiles was completely in contact with the steel block during testing.

With this surface modification, it was observed that the out-of-plane displacements in the X direction were ~35db lower than the respective in-plane displacements, whereas before this surface modification the gain difference was only ~10db, especially at low frequency. The gain difference for actuation in the Y direction was ~20dB for the relevant interaction with the Z and X axis as shown in Figure 18 (b). This is mainly because the piezo actuators in the Y-direction are not as well aligned as the Piezo actuators in the X direction.

Custom alignment of the piezo actuators

It is clearly desirable to make both the X and Y dynamics as identical as possible in order to minimize interaction due to the relevant piezo-actuators. This simplifies the control problem to single-input-single-output structures for high-speed-stage operation. From the analysis of the results shown in Figure 18, alignment of the piezo-actuators needs to be carried out. Identical piezo actuator aligners were 3D-printed.

(a) Frequency Plot : XX, XY and XZ



(b) Frequency Plot : YY, YX and YZ

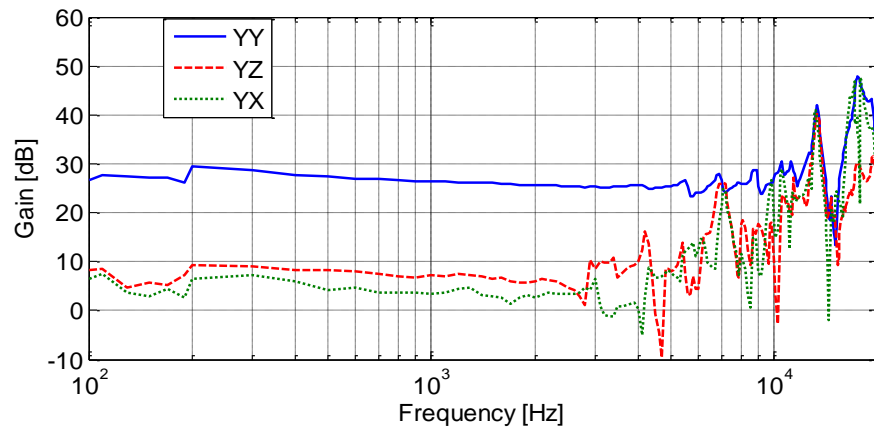


Fig. 18: Improved performance [nm/V] of the high-speed-stage after levelling the foot profiles

Piezo actuators and side clamps fixed

In order to obtain consistent high-speed-stage performance in terms of displacements and out-of-plane vibrations, it was decided to leave piezo-actuator aligners to firmly hold the respective piezo actuators at the required position of the high-speed-stage. This prevented the piezo actuators from dislocating themselves due to gravity and successive testing. To avoid the bolts from loosening, the side clamps were tightened after the bolt preloads are set by a digital torque wrench and hot glue has been applied as shown in Figure 19. This prevents any oscillatory movement of the side clamps.

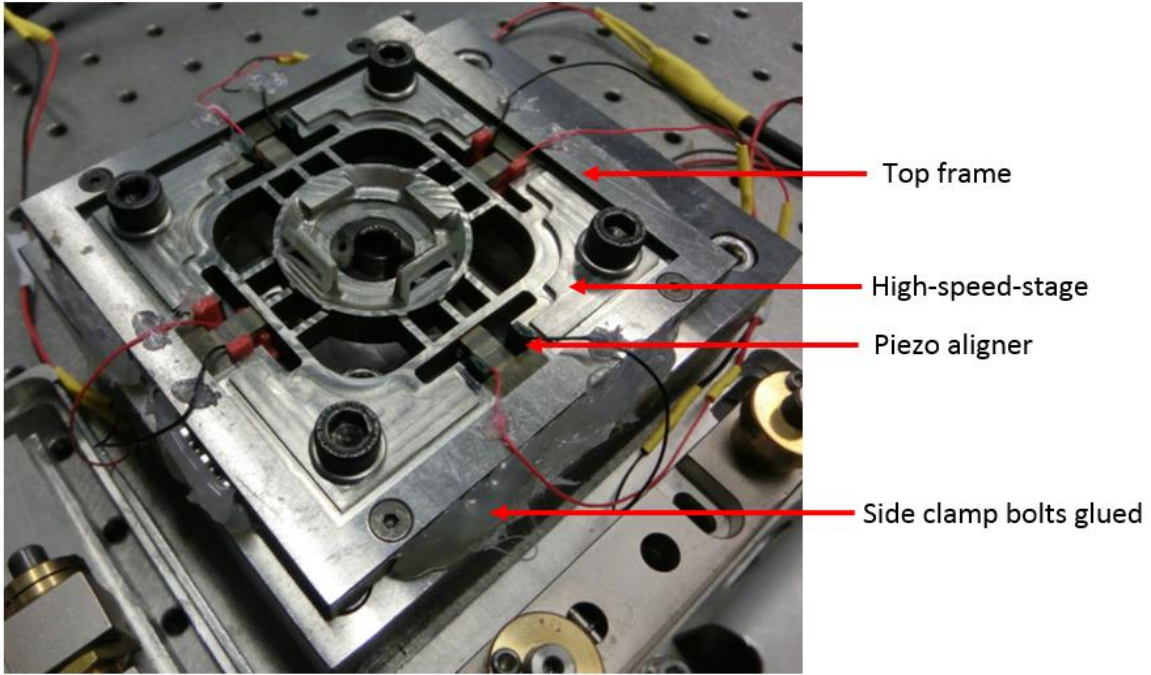


Fig. 19: High speed stage after all the post manufacturing modifications

5.4. Test results after modifications

The modifications mentioned in Section 5.3 were carried out on the high-speed-stage until the desired performance, as seen by the frequency plots of Figure 20, was obtained.

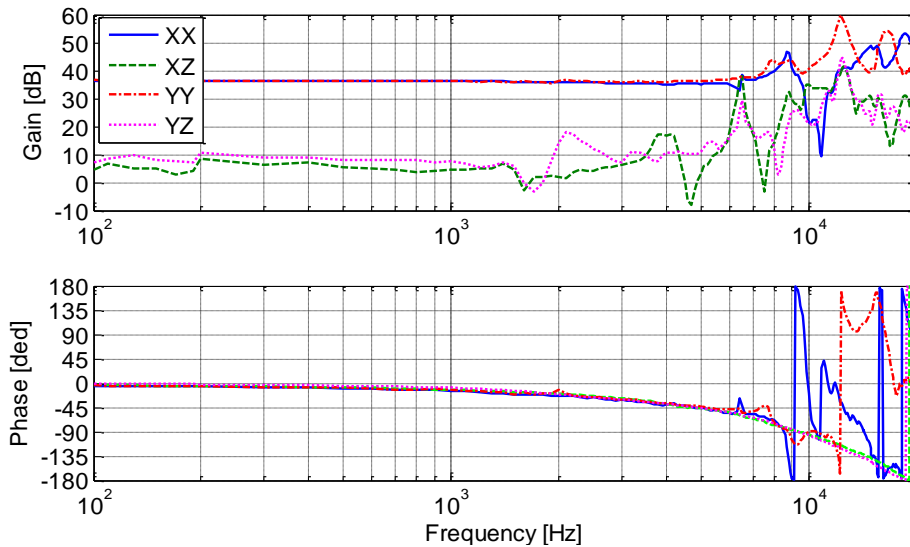


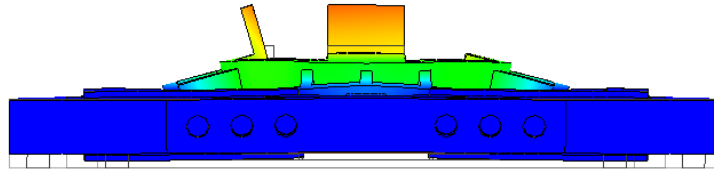
Fig. 20: Performance [nm/V] of the high-speed-stage upon post manufacturing optimisation

This process provides matching dynamics of both the X and Y directions. The low frequency gains of both X to X and Y to Y motion are now identical at an increased value of $\sim -25\text{dB}$. Hence, for a motion of $1\ \mu\text{m}$ in-plane motion there is an out-of-plane motion of just $0.056\ \mu\text{m}$. This is possible because the controllers are suppressing the resonance frequency through a fast drop in controller gain at high frequency.

The gain difference for the out-of-plane displacement frequency responses in relation to their respective in-plane displacement frequency behaviour have been set to a value of $\sim 25\text{dB}$ at low frequency. The out-of-plane displacements gradually increase near $6\ \text{kHz}$. This frequency was identified as the high-speed-stage's first resonance after all the post manufacturing modifications. This frequency is around one kHz lower than the $\sim 7.3\ \text{kHz}$ observed during FEA.

It is known that the first mode shape of a vibrating plate consists of a single peak with nodes at the restrained boundaries. This is seen by the modal analysis of the high-speed-stage during FEA. Therefore, it was understood why the out-of-plane displacements increased rapidly compared to its in-plane displacements at about $6\ \text{kHz}$ of the actual high-speed-stage, as our point of measurement of out-of-plane displacement is at the inner edge of the centre part (the first mode shape of the high-speed-stage is shown in Figure 21).

(a) Side view of the high-speed-stage's first mode shape



(b) High-speed-stage's first mode shape

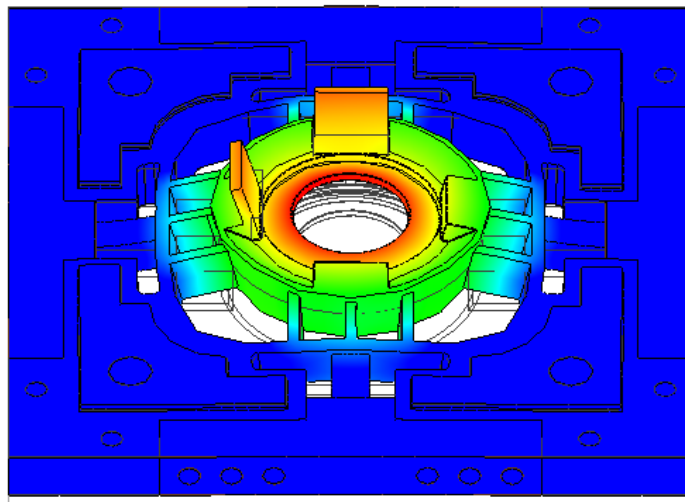


Fig. 21: First mode of the high-speed-stage as seen during FEA

6. Prototype 2 closed-loop control tests

6.1. Controller design

The overall implementation setup and the controller design are only briefly described to retain focus on the mechanical design aspects within the limits of this paper. Figure 22 shows the high-speed-stage system configuration (HS-NPS = High speed nano-positioning stage).

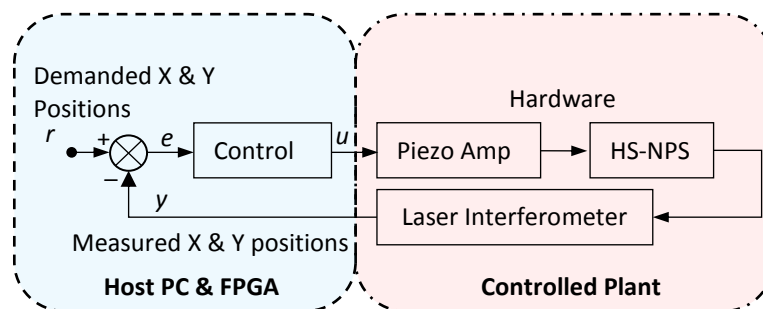


Fig. 22: Control loop structure

The high-speed-stage, the high-bandwidth piezo amplifier and the laser interferometer are treated as the controlled plant. The measured stage displacements in the X- and Y-axes are fed back to an FPGA based control implementation system from National Instruments (PXI-7854R) which can provide fast parallel computations and time-deterministic operation. The demanded stage positions, filters and the controllers were implemented on this FPGA board with a sample frequency of 100kHz. Based on the identified X and Y stage dynamics, the closed-loop controllers were designed in order to minimize the tracking errors, piezo nonlinearity, disturbances and the oscillatory behavior due to the excitations of the stage resonances at ~6.5kHz and ~9kHz. The open-loop frequency response which includes the stage and the controller dynamics in the X-axis is plotted in Figure 23.

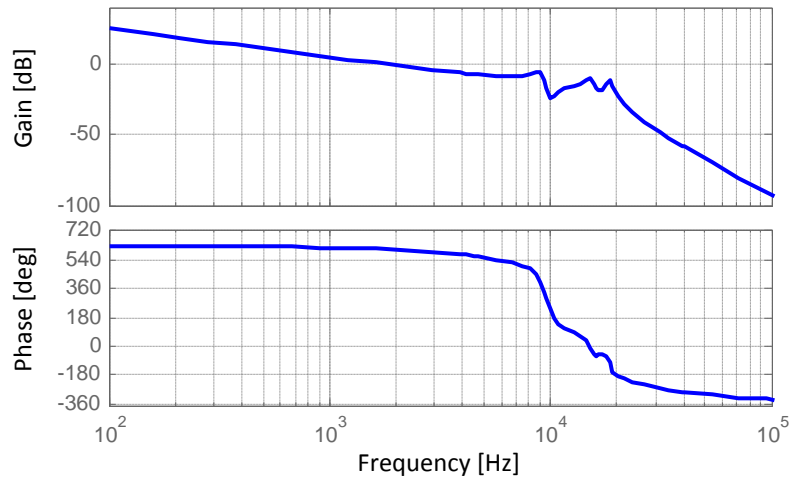


Fig. 23: Open-loop dynamics in the X-axis. Gain margin: 8.61dB at 5.83kHz, Phase margin: 65.3deg at 1.73kHz.

The frequency-shaped controller is of 4th order so that it does not consume the space of the FPGA. The gain and phase margins (Gain margin and Phase margin) of this open-loop system are 8.61dB and 65.3degrees, respectively. Hence this guarantees a robust and stable closed-loop system. Note that the controller for the Y-axis was designed in a similar manner and so the corresponding bode plot is omitted for the sake of brevity.

6.2. Comparative implementation tests results

To verify the performance of the designed controller, comparative benchmark tests (i.e. with and without the controller) were carried out. The time-series data in the X-axis of the high-speed-stage are shown in Figure 24. The blue dashed-line is the demanded position signal, the green dash-dotted line provides the results for an open-loop configuration (i.e. without control) and the red solid-line is the result for closed-loop (i.e. with the controller) responses. As seen from Figure 24(a), large overshoots, steady-state errors and oscillatory responses were observed for the stage without the controller. Furthermore, its response also drifts due to the piezo hysteresis. This can cause a distorted scanned image.

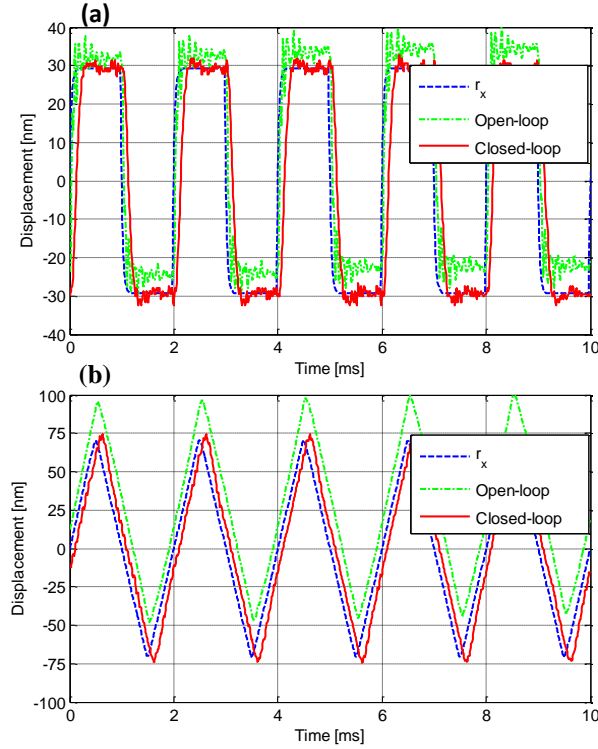


Fig. 24: Positioning performance with and without control: (a) Square wave (b) Triangular wave tests.

On the other hand, with the controller, stable and accurate tracking were maintained without the drift issue. In addition, a settling time of $\sim 0.4\text{ms}$ was achieved. Figure 24(b) shows the test result for a triangular wave demand at 500Hz . The open-loop controller does not work well due to the piezo drift, however the closed-loop strategy shows a satisfactory demand signal following performance. The frequency responses of the in-plane (XX) and the out-of-plane (XZ) dynamics with/without the controller are also presented in Figure 25.

The stage resonances at $\sim 6.5\text{kHz}$ and $\sim 9\text{kHz}$ are successfully compensated by the controller. The controller is a single input single output controller that acts as a low-pass filter. In this case, a closed-loop bandwidth of $\sim 2\text{kHz}$ has been obtained. Moreover, noticeable out-of-plane dynamics in the high-frequency region are also reduced. Thus, the high-speed-stage together with this controller can achieve precise high-speed scanning. Note that the Y-axis test data are omitted in this paper since the results in the Y-axis are similar to those of the X-axis due to the symmetric structure of the high-speed-stage.

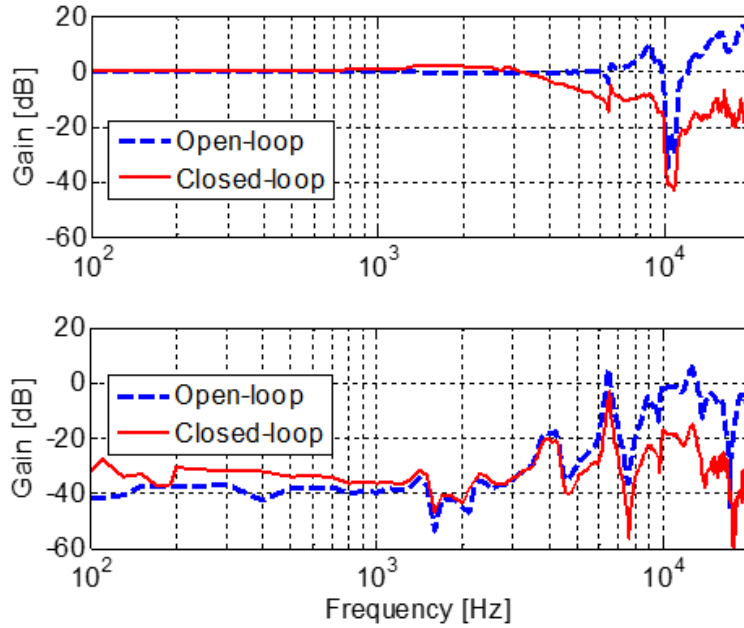


Fig. 25: The in-plane (XX-dynamics) and the out-of-plane (XZ-dynamics) responses in the frequency domain.

7. Conclusions

A bespoke high-speed positioning stage has been designed for a transverse dynamic force microscope (TDFM). An overall resonance frequency of over 6 kHz was achieved allowing a closed loop-control frequency of 1.73 kHz for precise horizontal motion control. This resonance represented a 12-fold increase from the original 500 Hz. The experimental out-of-plane distortions were reduced from 0.3 micron to 0.05microns. This level of performance gives good levels of accuracy and scan speeds for the TDFM. The scanning speed is approximately 250 $\mu\text{m/s}$.

As with most optimisation studies some key trade-offs were identified and resolved. One key trade-off involved the stiffness of the central dish holder. This part had to be stiff enough to prevent sliding of the dish but not so bulky that the overall resonance was too high. Another key trade-off involved achieving the right balance between high frequency and low-out-of plane distortions.

FEM modelling speeded up the optimisation process by revealing the relative effects of minor design changes. Practical testing proved to be essential because it identified problems that could not have been found in FEM modelling alone. In particular, practical testing revealed a lack of flatness in the bolted interface and also misalignment of the actuators.

References

- [1] Binnig, G. Quate, C. and Gerber, C., 1986, "Atomic force microscope," *Physical Review Letters*.
- [2] Hansma P.K., Schitter G., Fantner G.E. & Prater C. (2006). High-Speed Atomic Force Microscopy. *Science*, 314.
- [3] Howland, R. and Benatar, L., 1993, "Practical Guide to Scanning Probe Microscopy". Park Scientific Instruments: Sunnyvale, CA, USA.
- [4] Xu, X., Melcher, J., and Raman, A., 2010, "Accurate force spectroscopy in tapping mode atomic force microscopy in liquids," *Physical Reviews B*, vol. 81, pp. 035 407–1–035 407–7.
- [5] García, R., Magerle, R., & Perez, R. (2007). Nanoscale compositional mapping with gentle forces. *Nature materials*, 6(6), 405-411.
- [6] Lekka, M., & Laidler, P. (2009). Applicability of AFM in cancer detection. *Nature nanotechnology*, 4(2), 72-72.
- [7] Hoh, J. H., & Hansma, P. K. (1992). Atomic force microscopy for high-resolution imaging in cell biology. *Trends in Cell Biology*, 2(7), 208-213.
- [8] Burnham, N. A. and Colton, R. J., 1989, "Measuring the nanomechanical properties and surface forces of materials using an atomic force microscope," *Journal of Vacuum Science Technology*.
- [9] Harniman, R. L., Vicary, J. A., Hörber, J. K. H., Picco, L. M., Miles, M. J., and Antognozzi, M., 2012, "Methods for imaging DNA in liquid with lateral molecular-force microscopy," *Nanotechnology*, vol. 23, no. 8, p. 085703.
- [10] Antognozzi, M., Humphris, A., and Miles, M., 2001, "Observation of molecular layering in a confined water film and study of the layers viscoelastic properties," *Applied Physics Letters*, vol. 78, no. 3, pp. 300–302.
- [11] Brunner, R., Marti, O., and Hollricher, O., 1999 , "Influence of environmental conditions on shearforce distance control in near-field optical microscopy," *Journal of Applied Physics*, vol. 86, pp. 7100–7106.
- [12] Fletcher, JM, Harniman, RL, Barnes, FRH, Boyle, AL, Collins, AM, Mantell, J, Sharp, TH, Antognozzi, M, Booth, PJ, Linden, N, Miles, MJ, Sessions, RB, Verkade, P & Woolfson, DN 2013, 'Self-assembling cages from coiled-coil peptide modules' *Science*, vol 340, no. 6132, pp. 595-599.
- [13] James, P. J., Antognozzi, M., Tamayo, J., McMaster, T. J., Newton, J. M., and Miles, M. J., 2001, "Interpretation of contrast in tapping mode AFM and shear force microscopy. a study of Nafion," *Langmuir*, vol. 17, no. 2, pp. 349–360.
- [14] Antognozzi, M., Ulcinas, A., Picco, L., Simpson, S. H., Heard, P. J., Szczelkun, M. D., Brenner, B. and Miles, M. J., 2008, "A new detection system for extremely small vertically mounted cantilevers," *Nanotechnology*, vol. 19, no. 38, p. 384002.
- [15] Schitter G., Astrom K.J., Dematini B., Fantner G.E. Turner K. Thurner P.J. & Hansma P.K., 2006, Design and Modeling of a High-speed Scanner for Atomic Force Microscopy. American Control Conference, Minneapolis, USA.
- [16] Physik Instrumente. (2015). Accessed 16 Dec 2015, from website: <http://www.physikinstrumente.com/product-detail-page/p-7332-p-7333-201200.html>.
- [17] Physik Instrumente. (2015). Accessed 16 Dec 2015, from website: <http://www.physikinstrumente.com/product-detail-page/p-915khds-201680.html>

- [18] Yong Y.K., Aphale S. S. & Moheimani S. O. R. (2009). Design, Identification, and Control of a Flexure-Based XY Stage for Fast Nanoscale Positioning, IEEE Transactions on Nanotechnology, 8, 1.
- [19] Polit S. & Dong J. (2010). Development of a High-Bandwidth XY Nanopositioning Stage for High-Rate Micro-/Nanomanufacturing. IEEE.
- [20] Physik Instrumente. (2015). Accessed 9 Feb 2015, from website:
<http://www.physikinstrumente.com/productdetail-page/p-882-p-888-100810.html>